PHYSICAL REVIEW B **86**, 085421 (2012)

Plasmons and Coulomb drag in Dirac-Schrödinger hybrid electron systems

Alessandro Principi,[1] Matteo Carrega,[1] Reza Asgari,[2,*] Vittorio Pellegrini,[1,†] and Marco Polini[1,‡]

[1]*National Enterprise for Nanoscience and Nanotechnology (NEST), Istituto Nanoscienze - Consiglio Nazionale delle Ricerche and Scuola Normale Superiore, I-56126 Pisa, Italy*

[2]*School of Physics, Institute for Research in Fundamental Sciences (IPM), Tehran 19395-5531, Iran*

(Received 18 June 2012; published 10 August 2012)

We show that the plasmon spectrum of an ordinary two-dimensional electron gas (2DEG) hosted in a GaAs heterostructure is significantly modified when a graphene sheet is placed on the surface of the semiconductor in close proximity to the 2DEG. Long-range Coulomb interactions between massive electrons and massless Dirac fermions lead to a set of optical and acoustic intrasubband plasmons. Here we compute the dispersion of these coupled modes within the random phase approximation, providing analytical expressions in the long-wavelength limit that shed light on their dependence on the Dirac velocity and Dirac-fermion density. We also evaluate the resistivity in a Coulomb-drag transport setup. These Dirac-Schrödinger hybrid electron systems are experimentally feasible and open research opportunities for fundamental studies of electron-electron interaction effects in two spatial dimensions.

DOI: 10.1103/PhysRevB.86.085421 PACS number(s): 71.45.−d, 71.45.Gm, 72.80.Vp, 71.10.−w

I. INTRODUCTION

Plasmons are ubiquitous high-frequency collective density oscillations of an electron liquid, which occur in metals and semiconductors.[1] Their importance across different fields of basic and applied physics is by now well established. They play, for example, a key role in plasmonics[2] and in the photodetection of far-infrared radiation based on field-effect transistors.[3,4]

Plasmons in doped graphene sheets (hereafter dubbed "Dirac plasmons") have been intensively investigated by electron energy-loss spectroscopy (EELS).[5] EELS, however, does not have the sufficient energy and wave-number resolution to address, for example, the impact of broken Galilean invariance on Dirac plasmons.[6] Moreover, its application is limited to the collective modes in the charge channel with no information on the spin degrees of freedom, since the method probes only the "loss" function [i.e., the imaginary part of the inverse dielectric function $\varepsilon(q,\omega)$]. Angle-resolved photoemission spectroscopy[7] and scanning tunneling spectroscopy[8] also give precious information on Dirac plasmons, albeit in a slightly indirect way. Finally, Dirac plasmons have been probed by engineering directly their coupling to far-infrared light in a number of intriguing ways.[9] In contrast, the application of inelastic light (Raman) scattering to probe plasmons in graphene, has been, so far, limited to the investigation of magnetoplasmons in high magnetic fields.[10]

The situation is very different for the case of plasmons in 2DEGs realized, for example, in GaAs/AlGaAs modulation-doped semiconductor heterostructures. Indeed, these excitations have been successfully studied, both in zero magnetic field and in the quantum Hall regime, by resonant inelastic light scattering.[11,12] This method has a much better energy resolution than EELS (typically below 0.1 meV) and can be straightforwardly generalized to probe spin excitations. The cross section for scattering of photons by the electronic subsystem is, however, tiny. An ingenious resonance condition can be used in a light scattering experiment to enhance this cross section dramatically.[12] The frequency of the incoming or scattered photon can indeed be tuned close to the semiconductor band gap (e.g., $\approx$1.5 eV for GaAs at low temperature) making the energy denominators appearing in second-order perturbation theory[13] small and thus yielding a much higher sensitivity to collective electronic modes.

Graphene[14] is a gapless material though, and thus presents immediately an obstacle for the application of resonant inelastic light scattering. The van Hove singularity at the M point of graphene's Brillouin zone can be used to achieve resonance,[15] although the band gap at the M point is in the ultraviolet region of the electromagnetic spectrum ($\approx$4 eV) where tunable lasers having the required small line width for resonant inelastic light scattering do not exist.

In this article we propose a hybrid double-layer system composed by a doped graphene sheet that is Coulomb coupled to an ordinary 2DEG in a GaAs/AlGaAs semiconductor heterostructure, as schematically illustrated in Fig. 1. We demonstrate that precious information on Dirac plasmons is encoded in the dispersion of the collective in-phase and out-of-phase plasmon excitations of this massless Dirac-Schrödinger hybrid system (MDSHS). These collective modes can in principle be probed via inelastic light scattering by exploiting, as explained above, the resonance condition offered by the GaAs band gap. In passing, we mention that a similar resonant enhancement mechanism has been recently observed in the case of the Raman phonon lines in epitaxial graphene on copper substrates with incident photon energies overlapping the copper substrate photoluminescence.[16] We also study transport in a MDSHS in a Coulomb-drag setup,[17] demonstrating that, in the low-temperature Fermi-liquid regime and at strong coupling, the drag resistivity displays an intriguing dependence on carrier densities and interlayer separation, which is different from that known[17] for coupled 2DEGs in semiconductor double quantum wells.

Our paper is organized as follows. In Sec. II we introduce the model Hamiltonian and some basic definitions. In Sec. III we present analytical and numerical results, obtained by means of the random phase approximation, for the collective plasmons modes of MDSHSs. Our main analytical results on the Coulomb-drag resistivity are summarized and discussed in

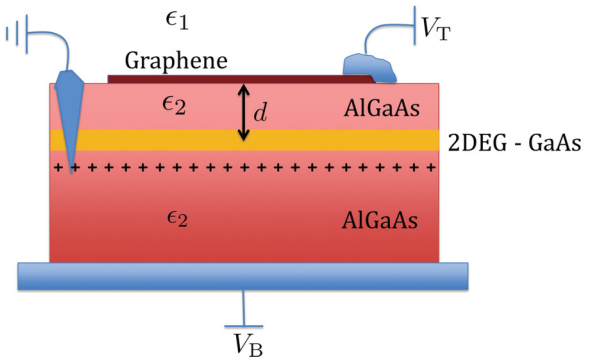

FIG. 1. (Color online) Schematics of the double-layer massless Dirac-Schrödinger hybrid electron system studied in this work. A graphene sheet is deposited on the surface of a semiconductor, underneath which a GaAs quantum well (at a distance d from the surface) hosts a high-mobility two-dimensional electron gas (2DEG). Carriers in the two layers are induced by conventional gating techniques (the + below the quantum well indicate the doping layer). In the presence of Coulomb coupling between the two subsystems, optical and acoustic hybrid collective modes emerge, which can be probed by resonant inelastic light scattering.

Sec. IV. Finally, in Sec. V we present a short summary of our main results accompanied by a discussion of the potential of MDSHSs.

II. MODEL HAMILTONIAN AND IMPORTANT DEFINITIONS

The system depicted in Fig. 1 can be modeled by the following Hamiltonian:

$$\begin{aligned}\hat{\mathcal{H}} = {} & \hbar v_{\rm D}\sum_{\boldsymbol{k},\alpha,\beta}\hat{\psi}^{\dagger}_{\boldsymbol{k},\alpha}(\boldsymbol{\sigma}_{\alpha\beta}\cdot\boldsymbol{k})\hat{\psi}_{\boldsymbol{k},\beta}+\frac{1}{2S}\sum_{\boldsymbol{q}\neq\boldsymbol{0}}V_{\rm tt}(q)\hat{\rho}^{\rm (t)}_{\boldsymbol{q}}\hat{\rho}^{\rm (t)}_{-\boldsymbol{q}}\\ & +\sum_{\boldsymbol{k}}\frac{\hbar^2\boldsymbol{k}^2}{2m_{\rm b}}\hat{\phi}^{\dagger}_{\boldsymbol{k}}\hat{\phi}_{\boldsymbol{k}}+\frac{1}{2S}\sum_{\boldsymbol{q}\neq\boldsymbol{0}}V_{\rm bb}(q)\hat{\rho}^{\rm (b)}_{\boldsymbol{q}}\hat{\rho}^{\rm (b)}_{-\boldsymbol{q}}\\ & +\frac{1}{2S}\sum_{\boldsymbol{q}}V_{\rm tb}(q)\left(\hat{\rho}^{\rm (t)}_{\boldsymbol{q}}\hat{\rho}^{\rm (b)}_{-\boldsymbol{q}}+\hat{\rho}^{\rm (b)}_{\boldsymbol{q}}\hat{\rho}^{\rm (t)}_{-\boldsymbol{q}}\right).\end{aligned}\tag{1}$$

The terms in the first and second lines of the previous equation describe two 2D electron systems with massless Dirac and parabolic Schrödinger bands, respectively. The last term describes Coulomb interactions between the two subsystems.

In the first line of Eq. (1), $v_{\rm D}$ is the Dirac velocity, $\boldsymbol{\sigma}=(\sigma^x,\sigma^y)$ is a 2D vector of Pauli matrices, S is the sample area, and $\hat{\psi}^{\dagger}_{\boldsymbol{k},\alpha}$ ($\hat{\psi}_{\boldsymbol{k},\alpha}$) creates (destroys) an electron with momentum $\boldsymbol{k}$ and sublattice-pseudospin index $\alpha=A,B$ in graphene. The Dirac density operator is defined by $\hat{\rho}^{\rm (t)}_{\boldsymbol{q}}=\sum_{\boldsymbol{k},\alpha}\hat{\psi}^{\dagger}_{\boldsymbol{k}-\boldsymbol{q},\alpha}\hat{\psi}_{\boldsymbol{k},\alpha}$. In the second line, $m_{\rm b}$ is the bare band mass of the 2DEG ($m_{\rm b}\approx 0.067m_{\rm e}$ in GaAs, $m_{\rm e}$ being the electron mass in vacuum), $\hat{\phi}^{\dagger}_{\boldsymbol{k}}$ ($\hat{\phi}_{\boldsymbol{k}}$) creates (destroys) an electron with momentum $\boldsymbol{k}$ in the 2DEG, and $\hat{\rho}^{\rm (b)}_{\boldsymbol{q}}=\sum_{\boldsymbol{k}}\hat{\phi}^{\dagger}_{\boldsymbol{k}-\boldsymbol{q}}\hat{\phi}_{\boldsymbol{k}}$ is the usual 2DEG density operator.

In writing Eq. (1) we have intentionally hidden "flavor" indices labeling spin and valley degrees-of-freedom in the graphene part of the Hamiltonian and spin degrees-of-freedom in the 2DEG part of the Hamiltonian. These flavors will just appear as degeneracy factors in the linear response functions $\chi_{\rm t}(q,\omega)$ and $\chi_{\rm b}(q,\omega)$, as we will see below. We have also completely neglected interlayer tunneling, which is strongly suppressed by the AlGaAs barrier between graphene and the quantum well.

The bare intralayer and interlayer Coulomb interactions, $V_{ij}(q)$ (with $i,j\in\{\rm t,b\}$), are influenced by the layered dielectric environment, modeled by two dielectric constants ϵ_1 and ϵ_2 in Fig. 1. A simple electrostatic calculation[18,19] implies that the Coulomb interaction in the graphene sheet (top layer) is given by $V_{\rm tt}(q)=4\pi e^2/[q(\epsilon_1+\epsilon_2)]$, The Coulomb interaction in the 2DEG (bottom layer) is instead

$$V_{\rm bb}(q)=\frac{4\pi e^2}{qD(q)}[(\epsilon_2+\epsilon_1)e^{qd}+(\epsilon_2-\epsilon_1)e^{-qd}],\tag{2}$$

where $D(q)=2\epsilon_2(\epsilon_1+\epsilon_2)e^{qd}$. Finally, the interlayer interaction is given by

$$V_{\rm tb}(q)=V_{\rm bt}(q)=\frac{8\pi e^2}{qD(q)}\epsilon_2.\tag{3}$$

Note that in the "uniform" $\epsilon_1=\epsilon_2\equiv\epsilon$ limit we recover the familiar expressions $V_{\rm tt}(q)=V_{\rm bb}(q)\to 2\pi e^2/(\epsilon q)$ and $V_{\rm tb}(q)=V_{\rm bt}(q)=V_{\rm tt}(q)\exp(-qd)$.

For the following analysis we introduce the electron density in the top (bottom) layer $n_{\rm t}$ ($n_{\rm b}$) and the corresponding Fermi wave numbers $k_{{\rm F},i}=\sqrt{4\pi n_i/N_i}$, where N_i is a degeneracy factor ($N_{\rm t}=4$ in the graphene layer and $N_{\rm b}=2$ in the 2DEG layer). We also introduce the Fermi energies $\varepsilon_{\rm F,t}=\hbar v_{\rm D}k_{\rm F,t}$ and $\varepsilon_{\rm F,b}=\hbar^2k^2_{\rm F,b}/(2m_{\rm b})$ in the top and bottom layers, respectively, $\alpha_{\rm ee}=e^2/(\hbar v_{\rm D})\approx 2.2$, and $r_s=(\pi n_{\rm b}a_{\rm B}^2)^{-1/2}$, $a_{\rm B}=\hbar^2/(m_{\rm b}e^2)$ being the Bohr radius calculated with the semiconductor band mass $m_{\rm b}$ (note the absence of any dielectric constant in the definition of $a_{\rm B}$).

III. COLLECTIVE OPTICAL AND ACOUSTIC PLASMON MODES

The collective modes of the system described by the Hamiltonian (1) can be determined[1] by locating the poles of the linear-response function $\boldsymbol{\chi}(q,\omega)$. Within the random phase approximation (RPA) these functions satisfy the following matrix equation:[1]

$$\boldsymbol{\chi}^{-1}(q,\omega)=\boldsymbol{\chi}_0^{-1}(q,\omega)-\boldsymbol{V}(q),\tag{4}$$

where $\boldsymbol{\chi}_0(q,\omega)$ is a 2×2 diagonal matrix whose elements $\chi_{\rm t}(q,\omega)$ and $\chi_{\rm b}(q,\omega)$ are the well-known noninteracting (Lindhard) response functions of each layer at arbitrary doping n_i. The mathematical and physical properties of $\chi_{\rm t}(q,\omega)$ are discussed in Ref. 20, while expressions for $\Re e[\chi_{\rm b}(q,\omega)]$ and $\Im m[\chi_{\rm b}(q,\omega)]$ can be found in Ref. 1. The off-diagonal (diagonal) elements of the matrix $\boldsymbol{V}=\{V_{ij}\}_{i,j=\rm t,b}$ represent interlayer (intralayer) Coulomb interactions.

A straightforward inversion of Eq. (4) yields the following condition for collective modes:

$$\begin{aligned}\varepsilon(q,\omega)=&[1-V_{\rm tt}(q)\chi_{\rm t}(q,\omega)][1-V_{\rm bb}(q)\chi_{\rm b}(q,\omega)]\\ &-V^2_{\rm tb}(q)\chi_{\rm t}(q,\omega)\chi_{\rm b}(q,\omega)=0.\end{aligned}\tag{5}$$

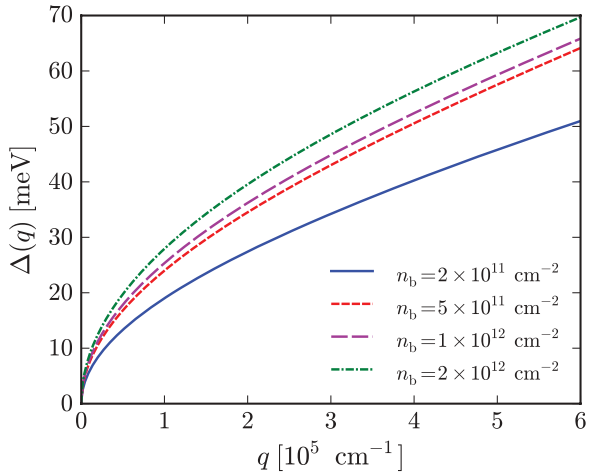

FIG. 2. (Color online) Optical plasmon dispersion in a massless Dirac-Schrödinger hybrid electron system. In this figure we plot the quantity $\Delta(q) = \hbar\omega_{\rm op}(q) - \hbar\omega_{\rm pl}(q)$ (in meV) as a function of the wave number q (in units of 10^5 cm^{-1}). Different line styles refer to different values of the 2DEG carrier density $n_{\rm b}$, ranging from $n_{\rm b} = 1\times10^{11}$ cm^{-2} to $n_{\rm b} = 1\times10^{12}$ cm^{-2}. The Dirac-fermion density is fixed at the value $n_{\rm t} = 10^{12}$ cm^{-2}, while the interlayer distance is $d = 30$ nm. With reference to Fig. 1, the dielectric constants have been fixed to $\epsilon_1 = 1$ and $\epsilon_2 = 13$. Note that $\Delta(q)$ is positive, implying a blue shift of the optical plasmon mode of the hybrid system with respect to the usual plasmon mode of an isolated 2DEG.

Zeroes of $\varepsilon(q,\omega)$ occur above the intraband particle-hole continuum where χ_i is real, positive, and a decreasing function of frequency. Equation (5) admits two solutions,[21] a higher-frequency solution at $\omega_{\rm op}(q\to0) \propto \sqrt{q}$, which corresponds to in-phase oscillations of the densities in the two layers (optical plasmon), and a lower-frequency solution at $\omega_{\rm ac}(q\to0) \propto q$, which corresponds to out-of-phase oscillations (acoustic plasmon).

A summary of our main results for $\omega_{\rm op}(q)$, obtained from the numerical solution of Eq. (5), is reported in Figs. 2 and 3. In these figures we plot the quantity $\Delta(q) = \hbar\omega_{\rm op}(q) - \hbar\omega_{\rm pl}(q)$, which physically represents the energy of the MDSHS optical plasmon measured from that of the plasmon of an *isolated* 2DEG, $\hbar\omega_{\rm pl}(q)$. We clearly see that $\Delta(q)$ is positive and $\approx$ 10 meV at $q \sim 10^5$ cm^{-1}.

To leading order in q in the long-wavelength $q\to0$ limit, the frequency of the MDSHS optical plasmon mode can be found analytically. The result is

$$\omega^2_{\rm op}(q\to0) = \left(\frac{N_{\rm t}e^2 v_{\rm D} k_{\rm F,t}}{2\hbar\bar\epsilon} + \frac{2\pi n_{\rm b}e^2}{m_{\rm b}\bar\epsilon}\right)q, \qquad (6)$$

where we have introduced $\bar\epsilon \equiv (\epsilon_1+\epsilon_2)/2$. We have checked that Eq. (6) is in perfect agreement with the numerical results displayed in Figs. 2 and 3. The first term on the right-hand side of Eq. (6) can be easily recognized[20] to be the square of the RPA plasmon frequency of the electron gas in an isolated graphene sheet separating two media with dielectric constants ϵ_1 and ϵ_2. The second term is the well-known RPA plasmon frequency of a 2D parabolic-band electron gas.[1] A measurement of $\omega_{\rm op}(q)$ in a MDSHS at sufficiently small q [more precisely, for $q \ll \min(k_{\rm F,t}, k_{\rm F,b})$] thus allows to access directly the Dirac velocity $v_{\rm D}$ and the Dirac-fermion density $n_{\rm t} \propto k^2_{\rm F,t}$.

In Fig. 4 we show illustrative results for the acoustic plasmon $\omega_{\rm ac}(q)$ as obtained from the numerical solution of Eq. (5) for different values of the 2DEG carrier densities $n_{\rm b}$. The dashed line in this figure represents the upper bound $\omega = v_{\rm D}q$ of the Dirac-fermion intraband electron-hole continuum.[20] Acoustic plasmon dispersions lying above the dashed line are not damped (within RPA) since they cannot decay by exciting intraband electron-hole pairs in the graphene sheet. When the dispersion hits the dashed line, Landau

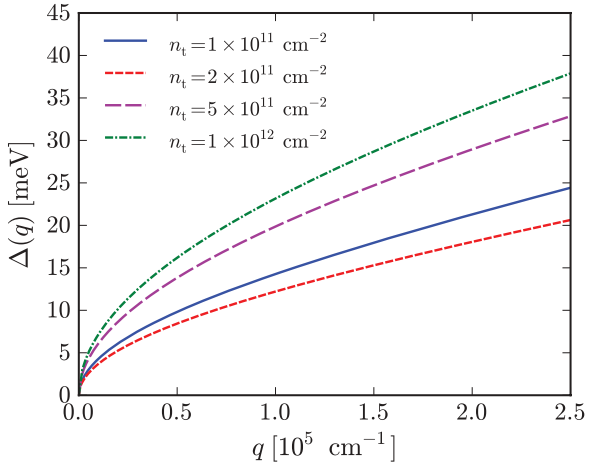

FIG. 3. (Color online) Same as in Fig. 2 but for different values of the Dirac-fermion density $n_{\rm t}$ and for a fixed value of the 2DEG carrier density $n_{\rm b} = 2\times10^{11}$ cm^{-2}. Notice the nonmonotonic behavior of $\Delta(q)$: for each q, $\Delta(q)$ reaches its minimum when the Dirac-fermion density matches the 2DEG density ($n_{\rm t} = n_{\rm b}$).

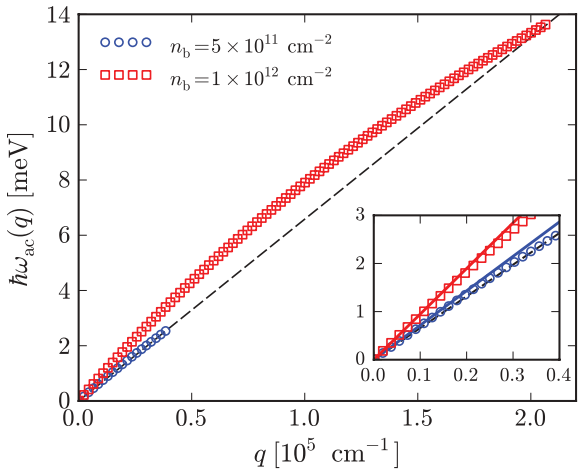

FIG. 4. (Color online) The acoustic plasmon mode of a massless Dirac-Schrödinger hybrid system. The acoustic plasmon dispersion $\hbar\omega_{\rm ac}(q)$ (in meV) is plotted as a function of the wave number q (in units of 10^5 cm^{-1}). Empty symbols label data for two different values of the 2DEG carrier density $n_{\rm b}$. In this figure we have fixed $n_{\rm t} = 1\times10^{11}$ cm^{-2} and $d = 60$ nm. The other parameters are identical to those used in Figs. 2 and 3. In the inset we illustrate the comparison between numerical results for the acoustic plasmon dispersion (empty symbols) and the analytical result $\omega_{\rm ac}(q\to0) = c_{\rm s}q$ (solid lines) with the velocity $c_{\rm s}$ obtained from the solution of Eq. (7). The dashed line marks the upper boundary of the Dirac fermion intraband single-particle continuum.

damping occurs and the acoustic plasmon pole acquires a finite lifetime. Note that when the 2DEG density is low (empty circles in Fig. 4) the acoustic-plasmon dispersion stays out of the Dirac-fermion intraband particle-hole continuum for a very small range of wave numbers q. It will be thus difficult to observe acoustic plasmons in MDSHSs in which the 2DEG carrier density is low.

The acoustic-plasmon group velocity $c_s = \lim_{q\to 0}\omega_{ac}(q)/q$ can be calculated analytically following the procedure explained in Ref. 22. After some tedious but straightforward algebra we find the following equation for $x = c_s/v_D$, the ratio between the acoustic-plasmon group velocity c_s and the Dirac velocity v_D:

$$2N_t\alpha_{ee}\xi\Gamma f(x)g(x) - \epsilon_2\Gamma g(x)\sqrt{x^2-1} - 2\epsilon_2 N_t\alpha_{ee} f(x)\sqrt{x^2 N_b r_s^2 - 4\alpha_{ee}^2} = 0, \quad (7)$$

where $\xi = dk_{F,t}$, $\Gamma = 2N_b/(k_{F,t}a_B)$, $f(x) = x - \sqrt{x^2-1}$, and $g(x) = x\sqrt{N_b}r_s - \sqrt{x^2 N_b r_s^2 - 4\alpha_{ee}^2}$. Note that the solution of Eq. (7) depends only on ϵ_2, while, as we have seen above, $\omega_{op}(q\to 0)$ depends on the average $\bar{\epsilon}$.

An undamped acoustic plasmon emerges for $x > x_{crit}$, where the threshold x_{crit} can be directly found from Eq. (7). When the Dirac velocity v_D is larger [smaller] than the Fermi velocity $v_{F,b} = \hbar k_{F,b}/m_b$ in the 2DEG, $x_{crit} = 1$ [$x_{crit} = v_{F,b}/v_D = 2\alpha_{ee}/(r_s\sqrt{N_b})$]. The existence of a solution of Eq. (7) thus depends on three parameters, namely d, n_t, and n_b (when the dielectric constants ϵ_1 and ϵ_2 are fixed). For example, given n_t and n_b, the acoustic plasmon emerges out of the continuum for $d > d^{(crit)}$ with

$$d^{(crit)} = \begin{cases} \dfrac{\epsilon_2\sqrt{N_b r_s^2 - 4\alpha_{ee}^2}}{\Gamma k_{F,t} g(1)}, & \text{if } v_D > v_{F,b} \\ \dfrac{\epsilon_2 v_{F,b}\sqrt{4\alpha_{ee}^2 - N_b r_s^2}}{4N_t\alpha_{ee}^2 v_D k_{F,t} f(v_{F,b}/v_D)}, & \text{otherwise} \end{cases}. \quad (8)$$

We remind the reader that the functions $f(x)$ and $g(x)$ have been defined right after Eq. (7). Similarly, given n_t and d, the acoustic plasmon emerges out of the continuum for $n > n_b^{(crit)}$, where

$$n_b^{(crit)} = \begin{cases} \dfrac{\epsilon_2 N_b(\epsilon_2 + 2\xi\Gamma)}{4\pi^2 a_B^2\alpha_{ee}^2(\epsilon_2+\xi\Gamma)^2}, & \text{if } v_D > v_{F,b} \\ \dfrac{N_b(\epsilon_2 + 2\xi N_t\alpha_{ee})^2}{4\pi\epsilon_2 a_B^2\alpha_{ee}^2(\epsilon_2 + 4\xi N_t\alpha_{ee})}, & \text{otherwise} \end{cases}. \quad (9)$$

Note that the critical values of d and n_b do not depend on n_t when $v_D > v_{F,b}$. They indeed depend only on the products $\Gamma k_{F,t}$ and $\xi\Gamma$, which are independent of $k_{F,t}$.

The theoretical prediction based on the solution of Eq. (7) is compared with the numerical results in the inset to Fig. 4.

We emphasize that the results summarized in Figs. 2–4 are directly amenable to experimental testing. Indeed, inelastic light scattering directly probes the dispersion of collective modes.[10–12] Finite values of the in-plane momentum q can be experimentally accessed by changing the angle θ_b between the incident-light beam and the sample: $q = 2\pi\cos(\theta_b)/\lambda_b$, where λ_b is the wavelength of the incident light.

IV. COULOMB-DRAG RESISTIVITY

In a drag experiment[17] a constant current is imposed on one layer (the "active" or "drive" layer). If no current is allowed to flow in the other one (the "passive" layer), an electric field develops, whose associated force cancels the frictional drag force exerted by the electrons in the active layer on the electrons in the passive one. The drag resistivity ρ_D, is defined as the ratio of the induced voltage in the passive layer to the applied current in the drive layer and reads $\rho_D = -\sigma_D/(\sigma_t\sigma_b - \sigma_D^2) \simeq -\sigma_D/(\sigma_t\sigma_b)$ in terms of the intralayer conductivities σ_t (σ_b) of the top (bottom) layer and the drag conductivity σ_D. Notice that in writing the last equality of the previous equation we have assumed $\sigma_D \ll \sigma_t, \sigma_b$.

Within the Kubo formalism the drag conductivity at the second order in the screened interlayer interaction $U_{tb}(q,\omega)$ reads[23] ($\hbar = 1$)

$$\sigma_D = \frac{\beta e^2}{8\pi}\int\frac{d^2\boldsymbol{q}}{(2\pi)^2}\int_0^\infty d\omega\frac{|U_{tb}(q,\omega)|^2}{\sinh^2(\beta\omega/2)}\Gamma_t(\boldsymbol{q},\omega)\Gamma_b(\boldsymbol{q},\omega), \quad (10)$$

where $\beta = (k_B T)^{-1}$ and $\Gamma_i(\boldsymbol{q},\omega)$ is the so-called nonlinear susceptibility of the ith layer. The dynamically screened interlayer interaction that appears in Eq. (10) is $U_{tb}(q,\omega) = V_{tb}(q)/\varepsilon(q,\omega)$, where $\varepsilon(q,\omega)$ is the RPA dielectric function defined in Eq. (5).

Here we focus only on the low-temperature limit [i.e., $k_B T \ll \min(\varepsilon_{F,t},\varepsilon_{F,b})$]. In this regime we can do the following approximations:[24] (i) use the low-temperature expressions for the intralayer conductivities σ_i, (ii) substitute $U_{tb}(q,\omega)$ in Eq. (10) with the statically screened interlayer interaction $U_{tb}(q,\omega=0)$, and (iii) expand the nonlinear susceptibilities $\Gamma_i(\boldsymbol{q},\omega\to 0)$ up to the lowest order in ω.

Following Ref. 24, we find the following results for the top layer (graphene sheet):

$$\lim_{T\to 0}\sigma_t = \frac{e^2}{4\pi}N_t\tau_t(k_{F,t})\varepsilon_{F,t} \quad (11)$$

and

$$\lim_{T\to 0}\Gamma_t(\boldsymbol{q},\omega\to 0) = -N_t\frac{\omega\tau_t(k_{F,t})}{2\pi v_D}\Theta(2k_{F,t}-q)\left(1-\frac{q^2}{4k_{F,t}^2}\right)^{1/2}\cos(\varphi_{\boldsymbol{q}}); \quad (12)$$

and the following results for the bottom layer (2DEG):

$$\lim_{T\to 0}\sigma_b = \frac{e^2}{2\pi}N_b\tau_b(k_{F,b})\varepsilon_{F,b} = \frac{n_b e^2\tau_b(k_{F,b})}{m_b} \quad (13)$$

and

$$\lim_{T\to 0}\Gamma_b(\boldsymbol{q},\omega\to 0) = -N_b\frac{\omega\tau_b(k_{F,b})}{4\pi v_{F,b}}\Theta(2k_{F,b}-q)\left(1-\frac{q^2}{4k_{F,b}^2}\right)^{-1/2}\cos(\varphi_{\boldsymbol{q}}), \quad (14)$$

where $v_{F,b}$ is the 2DEG Fermi velocity. Note the singularity at $q = 2k_{F,b}$ in the nonlinear susceptibility in Eq. (14). On the contrary, $\Gamma_t(\boldsymbol{q},\omega\to 0)$ vanishes at $q = 2k_{F,t}$, as a consequence of the absence of backscattering for massless Dirac fermions.[14]

Using Eqs. (11)–(14) we find that the drag resistivity in the low-temperature limit is given by

$$\lim_{T\to 0}\rho_{\rm D} = -\frac{1}{24e^2}\frac{1}{v_{\rm D}v_{\rm F,b}}\frac{(k_{\rm B}T)^2}{\varepsilon_{\rm F,t}\varepsilon_{\rm F,b}}\int_0^{q_{\rm max}} qdq|U_{\rm tb}(q,0)|^2 \times \mathcal{F}\left(\frac{q}{2k_{\rm F,t}},\frac{q}{2k_{\rm F,b}}\right), \tag{15}$$

where $q_{\rm max} = \min(2k_{\rm F,t},2k_{\rm F,b})$ and $\mathcal{F}(x,y) = \sqrt{(1-x^2)/(1-y^2)}$.

It is convenient at this stage to introduce a dimensionless expansion parameter $\eta \equiv d\sqrt{k_{\rm F,t}k_{\rm F,b}}$. The MDSHS is weakly (strongly) coupled if $\eta \gg 1$ ($\eta \ll 1$). Similar reasoning to that employed in Ref. 24 yields the following result for $\rho_{\rm D}$ in the weak-coupling limit (restoring Planck's constant for clarity):

$$\lim_{\eta\to\infty}\lim_{T\to 0}\rho_{\rm D} = -\frac{h}{e^2}\frac{\pi\zeta(3)\epsilon_2^2}{16\alpha_{\rm ee}^2N_{\rm t}^2N_{\rm b}^2}\frac{(k_{\rm B}T)^2}{\hbar^2v_{\rm D}^2k_{\rm F,t}^3k_{\rm F,b}^3d^4} \propto -\frac{h}{e^2}\frac{T^2}{n_{\rm t}^{3/2}n_{\rm b}^{3/2}d^4}. \tag{16}$$

We emphasize that the functional dependence of $\rho_{\rm D}$ on the carrier densities n_i and on the interlayer distance d in this limit is the same as in the case of two 2DEGs[25] and two graphene sheets.[24,26]

In the strong-coupling limit, we find

$$\lim_{\eta\to 0}\lim_{T\to 0}\rho_{\rm D} = -\frac{h}{e^2}\frac{\pi}{3}\alpha_{\rm ee}^2\frac{v_{\rm D}}{v_{\rm F,b}}\frac{(k_{\rm B}T)^2}{\varepsilon_{\rm F,t}\varepsilon_{\rm F,b}}\int_0^{x_{\rm max}} dx\,x \times \frac{\mathcal{F}\left(\sqrt{\frac{k_{\rm F,b}}{k_{\rm F,t}}}\frac{x}{2},\sqrt{\frac{k_{\rm F,t}}{k_{\rm F,b}}}\frac{x}{2}\right)}{[2\bar{\epsilon}x + 2(q_{\rm TF,t}+q_{\rm TF,b})/\sqrt{k_{\rm F,t}k_{\rm F,b}}]^2}, \tag{17}$$

where $x_{\rm max} = \min(2\sqrt{k_{\rm F,t}/k_{\rm F,b}},2\sqrt{k_{\rm F,b}/k_{\rm F,t}})$ and we have introduced the Thomas-Fermi screening wave numbers $q_{\rm TF,t} = N_{\rm t}\alpha_{\rm ee}k_{\rm F,t}$ and $q_{\rm TF,b} = N_{\rm b}^{3/2}r_sk_{\rm F,b}/2$.

The quadrature on the right-hand side of Eq. (17) can be carried out analytically in the special case $k_{\rm F,t} = k_{\rm F,b}$. Due to the different degeneracies in two layers, this condition implies a density imbalance between the two layers: $n_{\rm b} = N_{\rm b}n_{\rm t}/N_{\rm t} \equiv n$. In this case, Eq. (17) yields

$$\lim_{\eta\to 0}\lim_{T\to 0}\rho_{\rm D}\big|_{k_{\rm F,t}=k_{\rm F,b}} = -\frac{h}{e^2}\frac{\pi}{12}\frac{v_{\rm D}}{v_{\rm F,b}}\frac{(k_{\rm B}T)^2}{\varepsilon_{\rm F,b}\varepsilon_{\rm F,t}}\frac{\alpha_{\rm ee}^2}{\bar{\epsilon}^2}\left\{\ln\left[1+\frac{2\bar{\epsilon}}{N_{\rm t}\alpha_{\rm ee}+N_{\rm b}^{3/2}r_s/2}\right] - \frac{2\bar{\epsilon}}{2\bar{\epsilon}+N_{\rm t}\alpha_{\rm ee}+N_{\rm b}^{3/2}r_s/2}\right\}. \tag{18}$$

Equations (15)–(18) are the most important results of this section.[27] As in the case of drag between two graphene sheets,[24] Eq. (18) does not depend on the interlayer distance d. In the limit $n \to 0$ it yields a dependence of $\rho_{\rm D}$ on carrier density of the form $\rho_{\rm D} \propto n^{-1}$, analogously to what was found by Carrega *et al.*[24] for two graphene sheets with equal density [note that in the limit $n \to 0$ one has to find the asymptotic behavior of the expression in curly brackets in Eq. (18) for $r_s \to \infty$]. Finally, we emphasize that Eq. (18) does not contain the well-known[17] $\ln(T)$ factor, which appears in the drag resistivity at strong coupling in the case of two 2DEGs in semiconductor double quantum wells. This factor, which stems from the contribution to drag from momenta q of the order of $2k_{\rm F}$, is suppressed in the present case by the absence of backscattering for massless Dirac fermions[14] [compare Eq. (12) with Eq. (14)].

V. SUMMARY AND DISCUSSION

In this work we have proposed that massless Dirac-Schrödinger hybrid double layers be used to probe Dirac plasmons in a graphene sheet by employing resonant inelastic light scattering.[12] A natural resonant condition in this system is offered by the band gap of the semiconductor (e.g., GaAs) hosting an ordinary parabolic-band 2D electron gas, thus bypassing the nontrivial issue of the absence of a gap in an isolated graphene sheet. We have demonstrated that information on Dirac plasmons can be extracted in a rather direct manner from the measurement of the optical plasmon mode of the hybrid double layer. The latter supports also a soft mode, which disperses linearly as a function of wave number and whose observation requires a sufficiently high electron density in the semiconductor quantum well. Finally, we have calculated the low-temperature Coulomb-drag resistivity in the Boltzmann-transport limit, showing that in the strong-coupling limit it displays a dependence on carrier densities that is not shared by conventional all-semiconductor double quantum wells.[17]

The system depicted in Fig. 1 is amenable to experimental investigations and paves the way for the study of many other intriguing phenomena. We expect, for example, that massless Dirac-Schrödinger hybrid double layers will display interesting correlated states (and associated transport anomalies) induced by interlayer interactions deep in the quantum Hall regime. Another very appealing subject of investigation could be "hybrid exciton condensates". Exciton condensates are elusive many-particle systems in which electron-hole pairs condense below a certain critical temperature in a coherent superfluid.[28] Double-layer structures are extremely useful to spatially separate electrons and holes in two different layers, thereby suppressing electron-hole recombination.[29] Realizing all-semiconductor-based electron-hole double layers is a rather difficult task.[30] In contrast, holes can be trivially induced in the graphene sheet depicted in Fig. 1 by gating techniques. Massless Dirac-Schrödinger hybrid double layers thus offer unprecedented opportunities to realize, probe, and manipulate electron-hole quantum liquids and, hopefully, hybrid exciton condensates at sufficiently low temperatures.

ACKNOWLEDGMENTS

Work in Pisa was supported by Ministero dell'Istruzione dell'Università e della Ricerca (MIUR) through the program "FIRB - Futuro in Ricerca 2010", Grant No. RBFR10M5BT ("Plasmons and terahertz devices in graphene"). We thank Allan MacDonald, Leonid Levitov, Vincenzo Piazza, Aron Pinczuk, and Giovanni Vignale for useful discussions.

*asgari@ipm.ir
†vp@sns.it
‡m.polini@sns.it

[1]G. F. Giuliani and G. Vignale, *Quantum Theory of the Electron Liquid* (Cambridge University Press, Cambridge, 2005).

[2]S. A. Maier, *Plasmonics: Fundamentals and Applications* (Springer, New York, 2007); M. I. Stockman, Phys. Today **64**, 39 (2011).

[3]M. Dyakonov and M. Shur, Phys. Rev. Lett. **71**, 2465 (1993); for a recent review see, e.g., W. Knap, M. Dyakonov, D. Coquillat, F. Teppe, N. Dyakonova, J. Lusakowski, K. Karpierz, M. Sakowicz, G. Valusis, D. Seliuta, I. Kasalynas, A. El Fatimy, Y. M. Meziani, and T. Otsuji, J. Infrared Millim. TeraHz Waves **30**, 1319 (2009).

[4]L. Vicarelli, M. S. Vitiello, D. Coquillat, A. Lombardo, A. C. Ferrari, W. Knap, M. Polini, V. Pellegrini, and A. Tredicucci, Nature Mater. (to be published), arXiv:1203.3232.

[5]T. Eberlein, U. Bangert, R. R. Nair, R. Jones, M. Gass, A. L. Bleloch, K. S. Novoselov, A. Geim, and P. R. Briddon, Phys. Rev. B **77**, 233406 (2008); Y. Liu, R. F. Willis, K. V. Emtsev, and T. Seyller, *ibid.* **78**, 201403(R) (2008); J. Lu, K. P. Loh, H. Huang, W. Chen, and A. T. S. Wee, *ibid.* **80**, 113410 (2009); Y. Liu and R. F. Willis, *ibid.* **81**, 081406(R) (2010); R. J. Koch, T. Seyller, and J. A. Schaefer, *ibid.* **82**, 201413(R) (2010); T. Langer, J. Baringhaus, H. Pfnür, H. W. Schumacher, and C. Tegenkamp, New J. Phys. **12**, 033017 (2010); C. Tegenkamp, H. Pfnür, T. Langer, J. Baringhaus, and H. W. Schumacher, J. Phys.: Condens. Matter **23**, 012001 (2011); S. Y. Shin, C. G. Hwang, S. J. Sung, N. D. Kim, H. S. Kim, and J. W. Chung, Phys. Rev. B **83**, 161403(R) (2011).

[6]S. H. Abedinpour, G. Vignale, A. Principi, M. Polini, W.-K. Tse, and A. H. MacDonald, Phys. Rev. B **84**, 045429 (2011).

[7]A. Bostwick, F. Speck, T. Seyller, K. Horn, M. Polini, R. Asgari, A. H. MacDonald, and E. Rotenberg, Science **328**, 999 (2010); A. L. Walter, A. Bostwick, K.-J. Jeon, F. Speck, M. Ostler, T. Seyller, L. Moreschini, Y. J. Chang, M. Polini, R. Asgari, A. H. MacDonald, K. Horn, and E. Rotenberg, Phys. Rev. B **84**, 085410 (2011).

[8]V. W. Brar, S. Wickenburg, M. Panlasigui, C.-H. Park, T. O. Wehling, Y. Zhang, R. Decker, C. Girit, A. V. Balatsky, S. G. Louie, A. Zettl, and M. F. Crommie, Phys. Rev. Lett. **104**, 036805 (2010).

[9]L. Ju, B. Geng, J. Horng, C. Girit, M. Martin, Z. Hao, H. A. Bechtel, X. Liang, A. Zettl, Y. Ron Shen, and F. Wang, Nature Nanotech. **6**, 630 (2011); Z. Fei, G. O. Andreev, W. Bao, L. M. Zhang, A. S. McLeod, C. Wang, M. K. Stewart, Z. Zhao, G. Dominguez, M. Thiemens, M. M. Fogler, M. J. Tauber, A. H. Castro-Neto, C.-N. Lau, F. Keilmann, and D. N. Basov, Nano Lett. **11**, 4701 (2011); H. Yan, X. Li, B. Chandra, G. Tulevski, Y. Wu, M. Freitag, W. Zhu, P. Avouris, and F. Xia, Nature Nanotech. **7**, 330 (2012); Z. Fei, A. S. Rodin, G. O. Andreev, W. Bao, A. S. McLeod, M. Wagner, L. M. Zhang, Z. Zhao, G. Dominguez, M. Thiemens, M. M. Fogler, A. H. Castro-Neto, C. N. Lau, F. Keilmann, and D. N. Basov, Nature (2012), doi: 10.1038/nature11253; J. Chen, M. Badioli, P. Alonso-Gonzalez, S. Thongrattanasiri, F. Huth, J. Osmond, M. Spasenovic, A. Centeno, A. Pesquera, P. Godignon, A. Zurutuza, N. Camara, J. Garcia de Abajo, R. Hillenbrand, and F. Koppens, Nature (2012), doi: 10.1038/nature11254; H. Yan, Z. Li, X. Li, W. Zhu, P. Avouris, and F. Xia, Nano Lett. **12**, 3766 (2012); H. Yan, F. Xia, Z. Li, and P. Avouris, arXiv:1205.6841.

[10]J. Yan, S. Goler, T. D. Rhone, M. Han, R. He, P. Kim, V. Pellegrini, and A. Pinczuk, Phys. Rev. Lett. **105**, 227401 (2010); C. Faugeras, M. Amado, P. Kossacki, M. Orlita, M. Kühne, A. A. L. Nicolet, Yu. I. Latyshev, and M. Potemski, *ibid.* **107**, 036807 (2011).

[11]A. Pinczuk, and G. Abstreiter, Light Scattering in Solids V, Topics in Applied Physics **66**, 153 (1989); C. F. Hirjibehedin, A. Pinczuk, B. S. Dennis, L. N. Pfeiffer, and K. W. West, Phys. Rev. B **65**, 161309 (2002).

[12]For a recent review see, for example, V. Pellegrini and A. Pinczuk, Phys. Status Solidi B **243**, 3617 (2006).

[13]V. B. Berestetskii, E. M. Lifshitz, and L. P. Pitaevskii, *Quantum Electrodynamics* (Pergamon Press, Oxford, 1982), ch. VI.

[14]A. K. Geim and K. S. Novoselov, Nature Mater. **6**, 183 (2007); M. I. Katsnelson and K. S. Novoselov, Solid State Commun. **143**, 3 (2007); A. K. Geim and A. H. MacDonald, Phys. Today **60**, 35 (2007).

[15]C.-F. Chen, C.-H. Park, B. W. Boudouris, J. Horng, B. Geng, C. Girit, A. Zettl, M. F. Crommie, R. A. Segalman, S. G. Louie, and F. Wang, Nature (London) **471**, 617 (2011).

[16]S. D. Costa, A. Righi, C. Fantini, Y. Hao, C. Magnuson, L. Colombo, R. S. Ruoff, and M. A. Pimenta, Solid State Commun. **152**, 1317 (2012).

[17]T. J. Gramila, J. P. Eisenstein, A. H. MacDonald, L. N. Pfeiffer, and K. W. West, Phys. Rev. Lett. **66**, 1216 (1991); for a review see A. G. Rojo, J. Phys.: Condens. Matter **11**, 31R (1999).

[18]R. E. V. Profumo, M. Polini, R. Asgari, R. Fazio, and A. H. MacDonald, Phys. Rev. B **82**, 085443 (2010); M. I. Katsnelson, *ibid.* **84**, 041407(R) (2011).

[19]A form factor related to the finite width of the quantum well where the 2DEG is hosted has been neglected for the sake of simplicity and has the effect of weakening $V_{\rm bb}(q)$. Its introduction does not pose any conceptual difficulty and does not change our results qualitatively.

[20]Kenneth W.-K. Shung, Phys. Rev. B **34**, 979 (1986); B. Wunsch, T. Stauber, F. Sols, and F. Guinea, New J. Phys. **8**, 318 (2006); V. Apalkov, X.-F. Wang, and T. Chakraborty, Int. J. Mod. Phys. B **21**, 1165 (2007); E. H. Hwang and S. Das Sarma, Phys. Rev. B **75**, 205418 (2007); M. Polini, R. Asgari, G. Borghi, Y. Barlas, T. Pereg-Barnea, and A. H. MacDonald, *ibid.* **77**, 081411(R) (2008); A. Principi, M. Polini, and G. Vignale, *ibid.* **80**, 075418 (2009); M. Jablan, H. Buljan, and M. Soljacic, *ibid.* **80**, 245435 (2009); T. Stauber, J. Schliemann, and N. M. R. Peres, *ibid.* **81**, 085409 (2010); S. Yuan, R. Roldán, and M. I. Katsnelson, *ibid.* **84**, 035439 (2011).

[21]S. Das Sarma and A. Madhukar, Phys. Rev. B **23**, 805 (1981).

[22]G. E. Santoro and G. F. Giuliani, Phys. Rev. B **37**, 937 (1988); A. Principi, R. Asgari, and M. Polini, Solid State Commun. **151**, 1627 (2011); R. E. V. Profumo, R. Asgari, M. Polini, and A. H. MacDonald, Phys. Rev. B **85**, 085443 (2012).

[23]See, e.g., A. Kamenev and Y. Oreg, Phys. Rev. B **52**, 7516 (1995).

[24]M. Carrega, T. Tudorovskyi, A. Principi, M. I. Katsnelson, and M. Polini, New J. Phys. **14**, 063033 (2012).

[25]K. Flensberg, Ben Yu-Kuang Hu, A.-P. Jauho, and J. M. Kinaret, Phys. Rev. B **52**, 14761 (1995).

[26]W.-K. Tse, Ben Yu-Kuang Hu, and S. Das Sarma, Phys. Rev. B **76**, 081401 (2007); B. N. Narozhny, *ibid.* **76**, 153409 (2007); M. I. Katsnelson, *ibid.* **84**, 041407(R) (2011); N. M. R. Peres, J. M. B. Lopes dos Santos, and A. H. Castro Neto, Europhys. Lett. **95**, 18001 (2011); E. H. Hwang, R. Sensarma, and S. Das Sarma, Phys. Rev. B **84**, 245441 (2011); B. N. Narozhny, M. Titov, I. V. Gornyi, and P. M. Ostrovsky, *ibid.* **85**, 195421 (2012); S. M. Badalyan and F. M. Peeters, arXiv:1204.4598; B. Amorim and N. M. R. Peres, J. Phys.: Condens. Matter **24**, 335602 (2012).

[27]Coulomb drag between massless Dirac and ordinary Schrödinger fermions has been recently studied by B. Scharf and A. Matos-Abiague, arXiv:1204.3385v2. Our results for $\lim_{T\to 0}\rho_{\rm D}$ are smaller than theirs by a factor $N_{\rm t}N_{\rm b}=8$.

[28]J. M. Blatt, K. W. Böer, and W. Brandt, Phys. Rev. **126**, 1691 (1962); L. V. Keldysh and A. N. Kozlov, Sov. Phys. JETP **27**, 521 (1968).

[29]Y. E. Lozovik and V. I. Yudson, Solid State Comm. **19**, 391 (1976).

[30]A. F. Croxall, K. Das Gupta, C. A. Nicoll, M. Thangaraj, H. E. Beere, I. Farrer, D. A. Ritchie, and M. Pepper, Phys. Rev. Lett. **101**, 246801 (2008); J. A. Seamons, C. P. Morath, J. L. Reno, and M. P. Lilly, *ibid*. **102**, 026804 (2009).